UNIVERSITY OF LEEDS

This is a repository copy of *Mass balance of the Greenland Ice Sheet from 1992 to 2018*.

White Rose Research Online URL for this paper:
http://eprints.whiterose.ac.uk/158669/

Version: Accepted Version

Article:
Shepherd, A orcid.org/0000-0002-4914-1299, Ivins, E, Rignot, E et al. (86 more authors) (2020) Mass balance of the Greenland Ice Sheet from 1992 to 2018. Nature, 579 (7798). pp. 233-239. ISSN 0028-0836

https://doi.org/10.1038/s41586-019-1855-2

©The Author(s). This is an author produced version of an article published in Geochemical Transactions. Uploaded in accordance with the publisher's self-archiving policy.

Reuse
Items deposited in White Rose Research Online are protected by copyright, with all rights reserved unless indicated otherwise. They may be downloaded and/or printed for private study, or other acts as permitted by national copyright laws. The publisher or other rights holders may allow further reproduction and re-use of the full text version. This is indicated by the licence information on the White Rose Research Online record for the item.

Takedown
If you consider content in White Rose Research Online to be in breach of UK law, please notify us by emailing eprints@whiterose.ac.uk including the URL of the record and the reason for the withdrawal request.

White Rose university consortium
Universities of Leeds, Sheffield & York

eprints@whiterose.ac.uk
https://eprints.whiterose.ac.uk/

Mass balance of the Greenland Ice Sheet from 1992-2018

The IMBIE Team*

Abstract

In recent decades the Greenland Ice Sheet has been a major contributor to global sea-level rise [1,2], and it is expected to be so in the future [3]. Although increases in glacier flow [4–6] and surface melting [7–9] have been driven by oceanic [10–12] and atmospheric [13,14] warming, the degree and trajectory of today's imbalance remain uncertain. Here we compare and combine 26 individual satellite measurements of changes in the ice sheet's volume, flow and gravitational potential to produce a reconciled estimate of its mass balance. Although the ice sheet was close to a state of balance in the 1990's, annual losses have risen since then, peaking at 335 ± 62 billion tonnes per year in 2011. In all, Greenland lost 3800 ± 339 billion tonnes of ice between 1992 and 2018, causing mean sea-level to rise by 10.6 ± 0.9 millimetres. Using three regional climate models, we show that reduced surface mass balance has driven 1971 ± 555 billion tonnes (52 %) of the ice loss owing to increased meltwater runoff. The remaining 1827 ± 538 billion tonnes (48 %) of ice loss was due to increased glacier discharge, which rose from 41 ± 37 billion tonnes per year in the 1990's to 87 ± 25 billion tonnes per year since then. Between 2013 and 2017, the total rate of ice loss slowed to 217 ± 32 billion tonnes per year, on average, as atmospheric circulation favoured cooler conditions [15] and as ocean temperatures fell at the terminus of Jakobshavn Isbræ [16]. Cumulative ice losses from Greenland as a whole have been close to the IPCC's predicted rates for their high-end climate warming scenario [17], which forecast an additional 70 to 130 millimetres of global sea-level rise by 2100 when compared to their central estimate.

Introduction

The Greenland Ice Sheet holds enough water to raise mean global sea level by 7.4 m [18]. Its ice flows to the oceans through a network of glaciers and ice streams [19], each with a substantial inland catchment [20]. Fluctuations in the mass of the Greenland Ice Sheet occur due to variations in snow accumulation, meltwater runoff, ocean-driven melting, and iceberg calving. In recent decades, there have been marked increases in air [21] and ocean [12] temperatures and reductions in summer cloud cover [22] around Greenland. These changes have produced increases in surface runoff [8], supraglacial lake formation [23] and drainage [24], iceberg calving [25], glacier terminus retreat [26], submarine melting [10,11], and ice flow [6], leading to widespread changes in the ice sheet surface elevation, particularly near its margin (Figure 1).

Over recent decades, ice losses from Greenland have made a significant contribution to global sea-level rise [2], and model projections suggest that this imbalance will continue in a warming climate [3]. Since the early 1990's there have been comprehensive satellite observations of changing ice sheet velocity [4,6], elevation [27–29] and, between 2002 and 2016, its changing gravitational attraction [30,31], from which complete estimates of Greenland Ice Sheet mass balance are determined [1]. Prior to the 1990's, only partial surveys of the ice sheet elevation [32] and velocity [33] change are available. In combination with models of surface mass balance (the net difference between precipitation, sublimation and meltwater runoff) and glacial isostatic adjustment [34], satellite measurements have shown a fivefold increase in the rate of ice loss from Greenland overall, rising from 51 ± 65 Gt/yr in the early 1990's to 263 ± 30 Gt/yr between 2005 and 2010 [1]. This ice loss has been driven by changes in surface mass balance [7,21] and ice dynamics [5,33]. There was, however, a marked reduction in ice loss between 2013 and 2018, as a consequence of cooler atmospheric conditions and increased

precipitation [15]. While the broad pattern of change across Greenland (Figure 1) is one of ice loss, there is considerable variability; for example, during the 2000's just 4 glaciers were responsible for half of the total ice loss due to increased discharge [5], whereas many others contribute today [33]. Moreover, some neighbouring ice streams have been observed to speed up over this period while others slowed down [35], suggesting diverse reasons for the changes that have taken place - including their geometrical configuration and basal conditions, as well as the forcing they have experienced [36]. In this study we combine satellite altimetry, gravimetry, and ice velocity measurements to produce a reconciled estimate of the Greenland Ice Sheet mass balance between 1992 and 2018, we evaluate the impact of changes in surface mass balance and uncertainty in glacial isostatic adjustment, and we partition the ice sheet mass loss into signals associated with surface mass balance and ice dynamics. In doing so, we extend a previous assessment [1] to include more satellite and ancillary data and to cover the period since 2012.

Data and Methods

We use 26 estimates of ice sheet mass balance derived from satellite altimetry (9 data sets), satellite gravimetry (14 data sets) and the input-output method (3 data sets) to assess changes in Greenland ice sheet mass balance. The satellite data were computed using common spatial [20,37] and temporal domains, and using a range of models to estimate signals associated with changes in surface mass balance and glacial isostatic adjustment. Satellite altimetry provides direct measurements of changing ice sheet surface elevation recorded at orbit crossing points [32], along repeated ground tracks [27], or using plane-fit solutions [28], and the ice sheet mass balance is estimated from these measurements either by prescribing the density of the elevation fluctuation [38] or by making an explicit model-based correction for changes in firn height [39]. Satellite gravimetry measures fluctuations in the Earth's gravitational field as computed using either global spherical harmonic solutions [30] or using spatially-discrete mass concentration units [31]. Ice sheet mass changes are determined after making model-based corrections for glacial isostatic adjustment [30]. The input-output method uses model estimates of surface mass balance [7], which comprises the input, and satellite observations of ice sheet velocity computed from radar [6] and optical [40] imagery combined with airborne measurements of ice thickness [33] to compute changes in marine-terminating glacier discharge into the oceans, which comprises the output. The overall mass balance is the difference between input and output. Not all annual surveys of ice sheet discharge are complete, and sometimes regional extrapolations have to be employed to account for gaps in coverage [33]. Because they provide important ancillary data, we also assess 6 models of glacial isostatic adjustment and 10 models of surface mass balance.

To compare and aggregate the individual satellite data sets, we first adopt a common approach to derive linear rates of ice sheet mass balance over 36-month intervals (see Methods). We then compute error-weighted averages of all altimetry, gravimetry, and input-output group mass trends, and we combine these into a single reconciled estimate of the ice sheet mass balance using error-weighting of the group trends. Uncertainties in individual rates of mass change are estimated as the root sum square of the linear model misfit and their measurement error, uncertainties in group rates are estimated as the root mean square of the contributing time-series errors, and uncertainties in reconciled rates are estimated as their root mean square error divided by the square root of the number of independent groups. Cumulative uncertainties are computed as the root sum square of annual errors, an approach that has been employed in numerous studies [1,17,33,41] and assumes that annual errors are not correlated over time. To improve on this assumption, it will be necessary to consider the covariance of the systematic and random errors present within each mass balance solution (see Methods).

Inter-comparison of satellite and model results

The satellite gravimetry and satellite altimetry data used in our assessment are corrected for the effects of glacial isostatic adjustment, although the correction is relatively small for altimetry as it appears as a change in elevation and not mass. The most prominent and consistent local signals of glacial isostatic adjustment among the 6 models we have considered are two instances of uplift peaking at about 5-6 mm/yr, one centered over northwest Greenland and Ellesmere Island, and one over northeast Greenland (see Methods and Extended Data Figure 3). Although some models identify a 2 mm/yr subsidence under large parts of the central and southern parts of the ice sheet, it is absent or of lower magnitude in others, which suggests it is less certain (Extended Data Table 1). The greatest difference among model solutions is at Kangerlussuaq Glacier in the southeast where a study [42] has shown that models and observations agree if a localized weak Earth structure associated with overpassing the Iceland hotspot is assumed; the effect is to offset earlier estimates of mass trends associated with glacial isostatic adjustment by about 20 Gt/yr. Farther afield, the highest spread between modelled uplift occurs on Baffin Island and beyond due to variations in regional model predictions related to the demise of the Laurentide Ice Sheet [42]. This regional uncertainty is likely a major factor in the spread across the ice-sheet-wide estimates. Nevertheless, at -3 ± 20 Gt/yr, the mass signal associated with glacial isostatic adjustment in Greenland shows no coherent substantive change and is negligible relative to reported ice sheet mass trends [1].

There is generally good agreement between the models of Greenland Ice Sheet surface mass balance that we have assessed for determining mass input - particularly those of a similar class; for example, 70% of all model estimated of runoff and accumulation fall within 1-sigma of their mean (see Methods and Extended Data Table 2). The exceptions are a global reanalysis with coarse spatial resolution that tends to underestimate runoff due to its poor delineation of the ablation zone, and a snow process model that tends to underestimate precipitation and to overestimate runoff in most sectors. Among the other 8 models, the average surface mass balance between 1980 and 2012 is 361 ± 40 Gt/yr, with a marked negative trend over time (Extended Data Figure 4) mainly due to increased runoff [7]. At regional scale, the largest differences occur in the northeast, where two regional climate models predict significantly less runoff, and in the southeast, where there is considerable spread in precipitation and runoff across all models. All models show high temporal variability in surface mass balance components, and all models show that the southeast receives the highest net intake of mass at the surface due to high rates of snowfall originating from the Icelandic Low [43]. By contrast, the southwest, which features the widest ablation zone [7], has experienced alternate periods of net surface mass loss and gain over recent decades, and has the lowest average surface mass balance across the ice sheet.

We assessed the consistency of the satellite altimetry, gravimetry, and input-output method estimates of Greenland Ice Sheet mass balance using common spatial and temporal domains (see Figure 2 and Methods). In general, there is close agreement between estimates determined using each approach, and the standard deviations of coincident altimetry, gravimetry, and input-output method annual mass balance solutions are 40, 30, and 22 Gt/yr, respectively (Extended Data Table 3). Once averages were formed for each technique, the resulting estimates of mass balance were also closely aligned (e.g. Extended Data Figure 6). For example, over the common period 2005 to 2015, the average Greenland Ice Sheet mass balance is -251 ± 63 Gt/yr and, by comparison, the spread of the altimetry, gravimetry, and input-output method estimates is just 24 Gt/yr (Extended Data Table 3). The estimated uncertainty of the aggregated mass balance solution (see Methods) is larger than the standard deviation of model corrections for glacial isostatic adjustment (20 Gt/yr for gravimetry) and for surface mass balance (40 Gt/yr), which suggests that their collective impacts

have been adequately compensated, and it is also larger than the estimated 30 Gt/yr mass losses from peripheral ice caps [44], which are not accounted for in all individual solutions. In keeping with results from Antarctica [41], rates of mass loss determined using the input-output method are the most negative, and those determined from altimetry are the least negative. However, the spread among the three techniques is 6 times lower for Greenland than it is for Antarctica [41], reflecting differences in the ice sheet size, the complexity of the mass balance processes, and limitations of the various geodetic techniques.

Ice sheet mass balance

We aggregated the average mass balance estimates from gravimetry, altimetry and the input-output method to form a single, time-varying record (Figure 2) and then integrated these data to determine the cumulative mass lost from Greenland since 1992 (Figure 3). Although Greenland has been losing ice throughout most of the intervening period, the rate of loss has varied significantly. Between 1992 and 2012, the rate of ice loss progressively increased, reaching a maximum of 335 ± 62 Gt/yr in 2011, ahead of the extreme summertime surface melting that occurred in the following year [14]. Since 2012, however, the trend has reversed, with a progressive reduction in the rate of mass loss during the subsequent period. By 2018 – the last complete year of our survey – the annual rate of ice mass loss had reduced to 111 ± 71 Gt/yr. The highly variable nature of ice losses from Greenland is a consequence of the wide range of physical processes that are affecting different sectors of the ice sheet [16,28,35], which suggests that care should be taken when extrapolating sparse measurements in space or time. Although the rates of mass loss we have computed between 1992 and 2011 are 18 % less negative than those of a previous assessment, which included far fewer data sets [1], the results are consistent given their respective uncertainties. Altogether, the Greenland Ice Sheet has lost 3800 ± 339 Gt of ice to the ocean since 1992, with roughly half of this loss occurring during the 6-year period between 2006 and 2012.

To determine the proportion of mass lost due to surface and ice dynamical processes, we computed the contemporaneous trend in Greenland Ice Sheet surface mass balance - the net balance between precipitation and ablation [7], which is controlled by interactions with the atmosphere (Figure 3). In Greenland, recent trends in surface mass balance have been largely driven by meltwater runoff [43], which has increased as the regional climate has warmed [13]. Because direct observations of ice sheet surface mass balance are too scarce to provide full temporal and spatial coverage [45], regional estimates are usually taken from atmospheric models that are evaluated with existing observations. Our evaluation (see Methods) shows that the finer spatial resolution regional climate models produce consistent results, likely due to their ability to capture local changes in melting and precipitation associated with atmospheric forcing, and to resolve the full extent of the ablation zone [46]. We therefore compare and combine estimates of Greenland surface mass balance derived from three regional climate models; RACMO2.3p2 [46], MARv3.6 [21] and HIRHAM [9]. To assess the surface mass change across the Greenland Ice Sheet between 1980 and 2018, we accumulate surface mass balance anomalies from each of the regional climate models (Extended Data Figure 7) and average them into a single estimate (Figure 3). Surface mass balance anomalies are computed with respect to the average between 1980 and 1990, which corresponds to a period of approximate balance [8] and is common to all models. In this comparison, all three models show that the Greenland Ice Sheet entered abruptly into a period of anomalously low surface mass balance in the late 1990's and, when combined, they show that the ice sheet lost 1971 ± 555 Gt of its mass due to meteorological processes between 1992 and 2018 (Table 1).

Just over half (52 %) of all mass losses from Greenland – and much of their short-term variability – have been due to variations in the ice sheet's surface mass balance and its indirect impacts on firn processes. For example, between 2007 and 2012, 71 % of the total ice loss (193 ± 37 Gt/yr) was due to surface mass balance, compared to 28 % (22 ± 20 Gt/yr) over the preceding 15 years and 58 % (139 ± 38 Gt/yr) since then (Table 1). The rise in the total rate of ice loss during the late-2000s coincided with warmer atmospheric conditions, which promoted several episodes of widespread melting and runoff [14]. The reduction in surface mass loss since then is associated with a shift of the North Atlantic Oscillation, which brought about cooler atmospheric conditions and increased precipitation along the southeastern coast [15]. Trends in the total ice sheet mass balance are not, however, entirely due to surface mass balance and, by differencing these two signals, we can estimate the total change in mass loss due to ice dynamical imbalance – i.e. the integrated, net mass loss from those glaciers whose velocity does not equal their long-term mean (Figure 3). Although this approach is indirect, it makes use of all the satellite observations and regional climate models included in our study, overcoming limitations in the spatial and temporal sampling of ice discharge estimates derived from ice velocity and thickness data. Our estimate shows that, between 1992 and 2018, Greenland lost 1827 ± 538 Gt of ice due to the dynamical imbalance of glaciers relative to their steady state, accounting for 48 % of the total imbalance (Table 1). Losses due to increased ice discharge rose sharply in the early 2000's when Jakobshavn Isbræ [10] and several other outlet glaciers in the southeast [47] sped up, and the discharge losses are now four times higher than in the 1990's. For a period between 2002 and 2007, ice dynamical imbalance was the major source of ice loss from the ice sheet as a whole, although the situation has since returned to be dominated by surface mass losses as several glaciers have slowed down [16].

Despite a reduction in the overall rate of ice loss from Greenland between 2013 and 2018 (Figure 2), the ice sheet mass balance remained negative, adding 10.6 ± 0.9 mm to global sea level since 1992. Although the average sea level contribution is 0.42 ± 0.08 mm/yr, the five-year average rate varied by a factor 5 over the 25-year period, peaking at 0.75 ± 0.08 mm/yr between 2007 and 2012. The variability in Greenland ice loss illustrates the importance of accounting for yearly fluctuations when attempting to close the global sea level budget [2]. Satellite records of ice sheet mass balance are also an important tool for evaluating numerical models of ice sheet evolution [48]. In their 2013 assessment, the Intergovernmental Panel on Climate Change (IPCC) predicted ice losses from Greenland due to surface mass balance and glacier dynamics under a range of scenarios, beginning in 2007 [17] (Figure 4). Although ice losses from Greenland have fluctuated considerably during the 12-year period of overlap between the IPCC predictions and our reconciled time series, the total change and average rate (0.69 mm/yr) are close to the upper range predictions (0.72 mm/yr), which implies a 70 to 130 mm of sea-level rise by the year 2100 above central estimates. The drop in ice losses between 2013 and 2018, however, shifted rates towards the lower end projections, and a longer period of comparison is required to establish whether the upper trajectory will continue to be followed. Even greater sea level contribution cannot be ruled out if feedbacks between the ice sheet and other elements of the climate system are underestimated by current ice sheet models [3]. Although the volume of ice stored in Greenland is a small fraction of that in Antarctica (12 %), its recent losses have been ~36 % higher [41] as a consequence of the relatively strong atmospheric [13,14] and oceanic [10,11] warming that has occurred in its vicinity, and its status as a major source of sea-level rise is expected to continue [3,17].

Conclusions

We combine 26 satellite estimates of ice sheet mass balance and assess 10 models of ice sheet surface mass balance and 6 models of glacial isostatic adjustment, to show that the Greenland Ice

Sheet lost 3800 ± 339 Gt of ice between 1992 and 2018. During the common period 2005 to 2015, the spread of mass balance estimates derived from satellite altimetry, gravimetry, and the input-output method is 24 Gt/yr, or 10% of the estimated rate of imbalance. The rate of ice loss has generally increased over time, rising from 18 ± 28 Gt/yr between 1992 to 1997, peaking at 270 ± 27 Gt/yr between 2007 and 2012, and reducing to 239 ± 20 Gt/yr between 2012 and 2017. Just over half (1971 ± 555 Gt, or 52 %) of the ice losses are due to reduced surface mass balance (mostly meltwater runoff) associated with changing atmospheric conditions [13,14], and these changes have also driven the shorter-term temporal variability in ice sheet mass balance. Despite variations in the imbalance of individual glaciers [4,5,33], ice losses due to increasing discharge from the ice sheet as a whole have risen steadily from 41 ± 37 Gt/yr in the 1990's to 87 ± 25 Gt/yr since then, and account for just under half of all losses (48 %) over the survey period.

Our assessment shows that estimates of Greenland Ice Sheet mass balance derived from satellite altimetry, gravimetry, and the input-output method agree to within 20 Gt/yr, that model estimates of surface mass balance agree to within 40 Gt/yr, and that model estimates of glacial isostatic adjustment agree to within 20 Gt/yr. These differences represent a small fraction (13 %) of the Greenland Ice Sheet mass imbalance and are comparable to its estimated uncertainty (13 Gt/yr). Nevertheless, there is still departure among models of glacial isostatic adjustment in northern Greenland. Spatial resolution is a key factor in the degree to which models of surface mass balance can represent ablation and precipitation at local scales, and estimates of ice sheet mass balance determined from satellite altimetry and the input-output method continue to be positively and negatively biased, respectively, compared to those based on satellite gravimetry (albeit by small amounts). More satellite estimates of ice sheet mass balance at the start (1990's) and end (2010's) of our record would help to reduce the dependence on fewer data during those periods; although new missions [49,50] will no doubt address the latter, further analysis of historical satellite data is required to address the former.

References

1. Shepherd, A. *et al.* A Reconciled Estimate of Ice-Sheet Mass Balance. *Science* **338**, 1183–1189 (2012).
2. WCRP Global Sea Level Budget Group. Global sea-level budget 1993–present. *Earth System Science Data* **10**, 1551–1590 (2018).
3. Pattyn, F. *et al.* The Greenland and Antarctic ice sheets under 1.5 °C global warming. *Nature Clim Change* **8**, 1053–1061 (2018).
4. Moon, T., Joughin, I., Smith, B. & Howat, I. 21st-Century Evolution of Greenland Outlet Glacier Velocities. *Science* **336**, 576–578 (2012).
5. Enderlin, E. M. *et al.* An improved mass budget for the Greenland ice sheet. *Geophysical Research Letters* **41**, 866–872 (2014).

6. Rignot, E. & Kanagaratnam, P. Changes in the Velocity Structure of the Greenland Ice Sheet. *Science* **311**, 986–990 (2006).
7. Broeke, M. van den *et al.* Partitioning Recent Greenland Mass Loss. *Science* **326**, 984–986 (2009).
8. Trusel, L. D. *et al.* Nonlinear rise in Greenland runoff in response to post-industrial Arctic warming. *Nature* **564**, 104–108 (2018).
9. Lucas-Picher, P. *et al.* Very high resolution regional climate model simulations over Greenland: Identifying added value. *Journal of Geophysical Research: Atmospheres* **117**, (2012).
10. Holland, D. M., Thomas, R. H., de Young, B., Ribergaard, M. H. & Lyberth, B. Acceleration of Jakobshavn Isbræ triggered by warm subsurface ocean waters. *Nature Geoscience* **1**, 659–664 (2008).
11. Seale, A., Christoffersen, P., Mugford, R. I. & O'Leary, M. Ocean forcing of the Greenland Ice Sheet: Calving fronts and patterns of retreat identified by automatic satellite monitoring of eastern outlet glaciers. *Journal of Geophysical Research: Earth Surface* **116**, (2011).
12. Straneo, F. & Heimbach, P. North Atlantic warming and the retreat of Greenland's outlet glaciers. *Nature* **504**, 36–43 (2013).
13. Hanna, E., Mernild, S. H., Cappelen, J. & Steffen, K. Recent warming in Greenland in a long-term instrumental (1881–2012) climatic context: I. Evaluation of surface air temperature records. *Environ. Res. Lett.* **7**, 045404 (2012).
14. Fettweis, X. *et al. Brief communication* 'Important role of the mid-tropospheric atmospheric circulation in the recent surface melt increase over the Greenland ice sheet'. *The Cryosphere* **7**, 241–248 (2013).
15. Bevis, M. *et al.* Accelerating changes in ice mass within Greenland, and the ice sheet's sensitivity to atmospheric forcing. *PNAS* **116**, 1934–1939 (2019).
16. Khazendar, A. *et al.* Interruption of two decades of Jakobshavn Isbrae acceleration and thinning as regional ocean cools. *Nat. Geosci.* **12**, 277–283 (2019).

17. Church, J. A. *et al.* Sea Level Change. in *Climate Change 2013: The Physical Science Basis. Contribution of Working Group I to the Fifth Assessment Report of the Intergovernmental Panel on Climate Change* (eds. Stocker, T. F. et al.) 1137–1216 (Cambridge University Press, 2013). doi:10.1017/CBO9781107415324.026.
18. Morlighem, M. *et al.* BedMachine v3: Complete Bed Topography and Ocean Bathymetry Mapping of Greenland From Multibeam Echo Sounding Combined With Mass Conservation. *Geophysical Research Letters* **44**, 11,051-11,061 (2017).
19. Joughin, I., Smith, B. E., Howat, I. M., Scambos, T. & Moon, T. Greenland flow variability from ice-sheet-wide velocity mapping. *Journal of Glaciology* **56**, 415–430 (2010).
20. Zwally, H. J., Giovinetto, M. B., Beckley, M. A. & Saba, J. L. Antarctic and Greenland drainage systems. (2012).
21. Fettweis, X. *et al.* Reconstructions of the 1900–2015 Greenland ice sheet surface mass balance using the regional climate MAR model. *The Cryosphere* **11**, 1015–1033 (2017).
22. Hofer, S., Tedstone, A. J., Fettweis, X. & Bamber, J. L. Decreasing cloud cover drives the recent mass loss on the Greenland Ice Sheet. *Science Advances* **3**, e1700584 (2017).
23. Leeson, A. A. *et al.* Supraglacial lakes on the Greenland ice sheet advance inland under warming climate. *Nature Climate Change* **5**, 51–55 (2015).
24. Palmer, S., McMillan, M. & Morlighem, M. Subglacial lake drainage detected beneath the Greenland ice sheet. *Nat Commun* **6**, 1–7 (2015).
25. Nick, F. M. *et al.* The response of Petermann Glacier, Greenland, to large calving events, and its future stability in the context of atmospheric and oceanic warming. *Journal of Glaciology* **58**, 229–239 (2012).
26. Joughin, I. *et al.* Ice-front variation and tidewater behavior on Helheim and Kangerdlugssuaq Glaciers, Greenland. *Journal of Geophysical Research: Earth Surface* **113**, (2008).
27. Pritchard, H. D., Arthern, R. J., Vaughan, D. G. & Edwards, L. A. Extensive dynamic thinning on the margins of the Greenland and Antarctic ice sheets. *Nature* **461**, 971–975 (2009).

28. McMillan, M. *et al.* A high-resolution record of Greenland mass balance. *Geophysical Research Letters* **43**, 7002–7010 (2016).
29. Sandberg Sørensen, L. *et al.* 25 years of elevation changes of the Greenland Ice Sheet from ERS, Envisat, and CryoSat-2 radar altimetry. *Earth and Planetary Science Letters* **495**, 234–241 (2018).
30. Velicogna, I. & Wahr, J. Greenland mass balance from GRACE. *Geophysical Research Letters* **32**, (2005).
31. Luthcke, S. B. *et al.* Recent Greenland Ice Mass Loss by Drainage System from Satellite Gravity Observations. *Science* **314**, 1286–1289 (2006).
32. Zwally, H. J., Bindschadler, R. A., Brenner, A. C., Major, J. A. & Marsh, J. G. Growth of Greenland Ice Sheet: Measurement. *Science* **246**, 1587–1589 (1989).
33. Mouginot, J. *et al.* Forty-six years of Greenland Ice Sheet mass balance from 1972 to 2018. *PNAS* **116**, 9239–9244 (2019).
34. Lecavalier, B. S. *et al.* A model of Greenland ice sheet deglaciation constrained by observations of relative sea level and ice extent. *Quaternary Science Reviews* **102**, 54–84 (2014).
35. King, M. D. *et al.* Seasonal to decadal variability in ice discharge from the Greenland Ice Sheet. *The Cryosphere* **12**, 3813–3825 (2018).
36. Porter, D. F. *et al.* Identifying Spatial Variability in Greenland's Outlet Glacier Response to Ocean Heat. *Front. Earth Sci.* **6**, (2018).
37. Rignot, E. & Mouginot, J. Ice flow in Greenland for the International Polar Year 2008–2009. *Geophysical Research Letters* **39**, (2012).
38. Sørensen, L. S. *et al.* Mass balance of the Greenland ice sheet (2003–2008) from ICESat data – the impact of interpolation, sampling and firn density. *The Cryosphere* **5**, 173–186 (2011).
39. Zwally, H. J. *et al.* Greenland ice sheet mass balance: distribution of increased mass loss with climate warming; 2003–07 versus 1992–2002. *Journal of Glaciology* **57**, 88–102 (2011).

40. Rosenau, R., Scheinert, M. & Dietrich, R. A processing system to monitor Greenland outlet glacier velocity variations at decadal and seasonal time scales utilizing the Landsat imagery. *Remote Sensing of Environment* **169**, 1–19 (2015).
41. The IMBIE Team. Mass balance of the Antarctic Ice Sheet from 1992 to 2017. *Nature* **558**, 219–222 (2018).
42. Khan, S. A. *et al.* Geodetic measurements reveal similarities between post–Last Glacial Maximum and present-day mass loss from the Greenland ice sheet. *Science Advances* **2**, e1600931 (2016).
43. Ettema, J. *et al.* Higher surface mass balance of the Greenland ice sheet revealed by high-resolution climate modeling. *Geophysical Research Letters* **36**, (2009).
44. Bolch, T. *et al.* Mass loss of Greenland's glaciers and ice caps 2003–2008 revealed from ICESat laser altimetry data. *Geophysical Research Letters* **40**, 875–881 (2013).
45. Vernon, C. L. *et al.* Surface mass balance model intercomparison for the Greenland ice sheet. *The Cryosphere* **7**, 599–614 (2013).
46. Noël, B. *et al.* Modelling the climate and surface mass balance of polar ice sheets using RACMO2 – Part 1: Greenland (1958–2016). *The Cryosphere* **12**, 811–831 (2018).
47. Howat, I. M., Joughin, I., Fahnestock, M., Smith, B. E. & Scambos, T. A. Synchronous retreat and acceleration of southeast Greenland outlet glaciers 2000–06: ice dynamics and coupling to climate. *Journal of Glaciology* **54**, 646–660 (2008).
48. Shepherd, A. & Nowicki, S. Improvements in ice-sheet sea-level projections. *Nature Climate Change* **7**, 672–674 (2017).
49. Markus, T. *et al.* The Ice, Cloud, and land Elevation Satellite-2 (ICESat-2): Science requirements, concept, and implementation. *Remote Sensing of Environment* **190**, 260–273 (2017).
50. Flechtner, F. *et al.* What Can be Expected from the GRACE-FO Laser Ranging Interferometer for Earth Science Applications? *Surv Geophys* **37**, 453–470 (2016).

Supplementary Information

This table is an excel spreadsheet
Supplementary Table 1 This table contains details of the satellite datasets used in this study.

Acknowledgements

This work is an outcome of the Ice Sheet Mass Balance Inter-Comparison Exercise (IMBIE) supported by the ESA Climate Change Initiative and the NASA Cryosphere Program. A.S. was additionally supported by a Royal Society Wolfson Research Merit Award and the UK Natural Environment Research Council Centre for Polar Observation and Modelling.

Author Contributions

A.S. and E.I. designed and led the study. E.R., B.S., M.v.d.B., I.V. and P.W. led the input–output-method, altimetry, surface mass balance (SMB), gravimetry and glacial isostatic adjustment (GIA) experiments, respectively. G.K., S.N., T.P., T.Sc. provided additional supervision on glaciology, K.B., A.H., I.J., M.E. and T.W. provided additional supervision on satellite observations, and N.S. provided additional supervision on GIA. G.M., M.E.P., and T.Sl. performed the mass balance data collation and analysis. T.Sl. performed the AR5 data analysis. P.W. and I.S. performed the GIA data analysis. M.v.W. and T.Sl. performed the SMB data analysis. A.S., E.I., K.B., M.E., N.G., A.H., H.K., M.M., I.O., I.S., T.Sl., M.v.W., and P.W. wrote the manuscript; A.S. led the writing, E.I., K.B., M.E., and T.Sl. led the drafting and editing, M.v.W. led the SMB text, P.W. and I.S. led the GIA text, and N.G., A.H., H.K., M.M., and I.O. contributed elsewhere. A.S., K.B., H.K., G.M., M.E.P, I.S., S.B.S., T.Sl., P.W., and M.v.W. prepared the figures and tables, with particular focus on Fig. 1 (S.B.S), Fig. 3 (T.Sl.), Fig. 4 (T.Sl.), Extended Data Fig. 2 (K.B.), Extended Data Fig. 3 (P.W.), Extended Data Fig. 2 (M.v.W.), Extended Data Table 1 (P.W. and I.S.), Extended Data Table 2 (M.v.W.), and Supplementary Table 1 (H.K. and T.Sl.); G.M. and M.E.P. led the production of all other figures and tables. All authors participated in the data interpretation and commented on the manuscript.

Competing Interests

The authors declare no competing interests.

The IMBIE Team

Andrew Shepherd[1*], Erik Ivins[2], Eric Rignot[2,3], Ben Smith[4], Michiel van den Broeke[5], Isabella Velicogna[2,3], Pippa Whitehouse[6], Kate Briggs[1], Ian Joughin[4], Gerhard Krinner[7], Sophie Nowicki[8], Tony Payne[9], Ted Scambos[10], Nicole Schlegel[2], Geruo A[3], Cécile Agosta[11], Andreas Ahlstrøm[12], Greg Babonis[13], Valentina R. Barletta[14], Anders A. Bjørk[15], Alejandro Blazquez[16], Jennifer Bonin[17], William Colgan[12], Beata Csatho[13], Richard Cullather[18], Marcus E. Engdahl[19], Denis Felikson[8], Xavier Fettweis[11], Rene Forsberg[14], Anna E. Hogg[1], Hubert Gallee[7], Alex Gardner[2], Lin Gilbert[20], Noel Gourmelen[21], Andreas Groh[22], Brian Gunter[23], Edward Hanna[24], Christopher Harig[25], Veit Helm[26], Alexander Horvath[27], Martin Horwath[22], Shfaqat Khan[14], Kristian K. Kjeldsen[12,28], Hannes Konrad[29], Peter L. Langen[30], Benoit Lecavalier[31], Bryant Loomis[8], Scott Luthcke[8], Malcolm McMillan[32], Daniele Melini[33],

Sebastian Mernild[34,35,36,37], Yara Mohajerani[3], Philip Moore[38], Ruth Mottram[30], Jeremie Mouginot[3,7], Gorka Moyano[39], Alan Muir[20], Thomas Nagler[40], Grace Nield[6], Johan Nilsson[2], Brice Noël[5], Ines Otosaka[1], Mark E. Pattle[39], W. Richard Peltier[41], Nadège Pie[42], Roelof Rietbroek[43], Helmut Rott[40], Louise Sandberg Sørensen[14], Ingo Sasgen[26], Himanshu Save[42], Bernd Scheuchl[3], Ernst Schrama[44], Ludwig Schröder[22,26], Ki-Weon Seo[45], Sebastian B. Simonsen[14], Thomas Slater[1], Giorgio Spada[46], Tyler Sutterley[3], Matthieu Talpe[2], Lev Tarasov[31], Willem Jan van de Berg[5], Wouter van der Wal[44, 47], Melchior van Wessem[5], Bramha Dutt Vishwakarma[48], David Wiese[2], David Wilton[49], Thomas Wagner[50], Bert Wouters[5,47] & Jan Wuite[40]

[1]Centre for Polar Observation and Modelling, University of Leeds, Leeds, UK. [2]NASA Jet Propulsion Laboratory, California Institute of Technology, Pasadena, CA, USA. [3]Department of Earth System Science, University of California, Irvine, CA, USA. [4]Department of Earth and Space Sciences, University of Washington, Seattle, WA, USA. [5]Institute for Marine and Atmospheric Research, Utrecht University, Utrecht, The Netherlands. [6]Department of Geography, Durham University, Durham, UK. [7]Institute of Environmental Geosciences, Université Grenoble Alpes, Grenoble, France. [8]Cryospheric Sciences Laboratory, NASA Goddard Space Flight Center, Greenbelt, MD, USA. [9]School of Geographical Sciences, University of Bristol, Bristol, UK. [10]Earth Science and Observation Center, University of Colorado, Boulder, CO, USA. [11]Department of Geography, University of Liège, Liège, Belgium. [12]Geological Survey of Denmark and Greenland, Copenhagen, Denmark. [13]Department of Geology, State University of New York at Buffalo, Buffalo, NY, USA. [14]DTU Space, National Space Institute, Technical University of Denmark, Kongens Lyngby, Denmark. [15]Department of Geosciences and Natural Resource Management, University of Copenhagen, Copenhagen, Denmark. [16]LEGOS, Université de Toulouse, Toulouse, France. [17]College of Marine Sciences, University of South Florida, Tampa, FL, USA. [18]Global Modeling and Assimilation Office, NASA Goddard Space Flight Center, Greenbelt, MD, USA. [19]ESA-ESRIN, Frascati, Italy. [20]Mullard Space Science Laboratory, University College London, Holmbury St Mary, UK. [21]School of Geosciences, University of Edinburgh, Edinburgh, UK. [22]Institute for Planetary Geodesy, Technische Universität Dresden, Dresden, Germany. [23]Daniel Guggenheim School of Aerospace Engineering, Georgia Institute of Technology, Atlanta, GA, USA. [24]School of Geography, University of Lincoln, Lincoln, UK. [25]Department of Geosciences, University of Arizona, Tucson, AZ, USA. [26]Alfred Wegener Institute, Helmholtz Centre for Polar and Marine Research, Bremerhaven, Germany. [27]Institute of Astronomical and Physical Geodesy, Technical University Munich, Munich, Germany. [28]GeoGenetics, Globe Institute, University of Copenhagen, Copenhagen, Denmark. [29]Deutscher Wetterdienst, Offenbach, Germany. [30]Danish Meteorological Institute, Copenhagen, Denmark. [31]Department of Physics and Physical Oceanography, Memorial University of Newfoundland, St. Johns, Newfoundland and Labrador, Canada. [32]University of Lancaster, Lancaster, UK. [34]Istituto Nazionale di Geofisica e Vulcanologia, Roma, Italy [34]Nansen Environmental and Remote Sensing Centre, Bergen, Norway. [35]Faculty of Engineering and Science, Western Norway University of Applied Sciences, Sogndal, Norway. [36]Direction of Antarctic and Sub-Antarctic Programs, Universidad de Magallanes, Punta Arenas, Chile, [37]Geophysical Institute, University of Bergen, Norway. [38]School of Engineering, Newcastle University, Newcastle upon Tyne, UK. [39]isardSAT, Barcelona, Spain. [40]ENVEO, Innsbruck, Austria. [41]Department of Physics, University of Toronto, Toronto, Ontario, Canada. [42]Center for Space Research, University of Texas, Austin, TX, USA. [43]Institute of Geodesy and Geoinformation, University of Bonn, Bonn, Germany. [44]Department of Space Engineering, Delft University of Technology, Delft, The Netherlands. [45]Department of Earth Science Education, Seoul National University, Seoul, South Korea. [46]Dipartimento di Scienze Pure e Applicate, Università di Urbino "Carlo Bo", Italy. [47]Department of Civil Engineering, Delft University of Technology, Delft, The Netherlands. [48]Geodetic Institute, Univerity of Stuttgart, Stuttgart, Germany. [49]Department of Computer Science, University of Sheffield, UK. [50]NASA Headquarters, Washington D.C., USA.

*Corresponding author: Andrew Shepherd a.shepherd@leeds.ac.uk

Figure and Table Legends

Figure 1 | Greenland Ice Sheet elevation change. Rate of elevation change of the Greenland Ice Sheet determined from ERS, ENVISAT, and CryoSat-2 satellite radar altimetry (top row) and from the HIRHAM5 surface mass balance model (bottom row, ice equivalent), over successive five-year epochs (left to right; 1992-1997, 1997-2002, 2002-2007, 2007-2012, 2012-2017). Reproduced from the data in Ref [29].

Figure 2 | Greenland Ice Sheet mass balance. Rate of mass change (dM/dt) of the Greenland Ice Sheet as determined from the satellite-altimetry (red), input-output method (blue) and gravimetry (green) assessments included in this study. In each case, dM/dt is computed at annual intervals from time series of relative mass change using a three-year window. An average of estimates across each class of measurement technique is also shown for each year (black). The estimated 1σ, 2σ and 3σ ranges of the class average is shaded in dark, mid and light grey, respectively; 97 % of all estimates fall within the 1σ range, given their estimated individual errors. The equivalent sea level contribution of the mass change is also indicated, and the number of individual mass-balance estimates collated at each epoch is shown below each chart entry.

Figure 3 | Cumulative anomalies in Greenland Ice Sheet total mass, surface mass balance and ice dynamics. The total change (dark blue) is determined as the integral of the average rate of ice sheet mass change (Figure 2). The change in surface mass balance (green) is determined from three regional climate models relative to their mean over the period 1980-1990. The change associated with ice dynamics (light blue) is determined as the difference between the change in total and surface mass. The estimated 1σ uncertainties of the cumulative changes are shaded. The dotted line shows the result of a previous assessment [1]. The equivalent sea level contribution of the mass change is also indicated. Vertical lines mark consecutive five-year epochs since the start of our satellite record in 1992.

Figure 4 | Observed and predicted sea level contribution due to Greenland Ice Sheet mass change. The global sea-level contribution from Greenland Ice Sheet mass change according to this study (black line) and IPCC AR5 projections between 1992–2040 (left) and 2040–2100 (right) including upper (red), mid (orange), and lower (blue) estimates from the sum of modelled surface mass balance and rapid ice dynamical contributions. Darker coloured lines represent pathways from the five AR5 scenarios in order of increasing emissions: RCP2.6, RCP4.5, RCP6.0, SRES A1B and RCP8.5. Shaded areas represent the spread of AR5 emissions scenarios and the 1σ estimated error on the IMBIE data. The bar chart plot (inset) shows the average annual rates of sea-level rise (in mm/yr) during the overlap period 2007–2018 and their standard deviations. Cumulative AR5 projections have been offset to make them equal to the observational record at their start date (2007).

Table 1 | Rates of Greenland Ice Sheet total, surface, and dynamical mass change. Total rates were determined from all satellite measurements over various epochs, rates of surface mass change were determined from three regional climate models, and rates of dynamical mass change were determined as the difference. The period 1992–2011 is included for comparison to a previous assessment [1], which reported a mass-balance estimate of -142 ± 49 Gt/yr based on far fewer data.

The small differences in our updated estimate is due to our inclusion of more data and an updated aggregation scheme (see Methods). Errors are 1σ.

Table 1

Region	1992-1997 (Gt/yr)	1997-2002 (Gt/yr)	2002-2007 (Gt/yr)	2007-2012 (Gt/yr)	2012-2017 (Gt/yr)	1992-2011 (Gt/yr)	1992-2018 (Gt/yr)
Total	-18 ± 28	-48 ± 35	-175 ± 30	-270 ± 27	-238 ± 29	-117 ± 16	-148 ± 13
Surface	26 ± 35	-15 ± 36	-78 ± 36	-193 ± 37	-139 ± 38	-57 ± 18	-76 ± 16
Dynamics	-43 ± 45	-33 ± 50	-97 ± 47	-77 ± 46	-100 ± 48	-60 ± 24	-73 ± 21

Methods

Data

In this assessment we analyse 5 groups of data: estimates of ice sheet mass-balance determined from 3 distinct classes of satellite observations - altimetry, gravimetry and the input–output method (IOM) - and model estimates of surface mass balance (SMB) and glacial isostatic adjustment (GIA). Each dataset is computed following previously reported methods (based on references 28, 33, 38, 54 to 61, 72, 87 to 120 and detailed in Supplementary Table 1) and, for consistency, they are aggregated within common spatial and temporal domains. Altogether, 26 separate ice sheet mass balance datasets were used - 9 derived from satellite altimetry, 3 derived from the input-output method, and 14 derived from satellite gravimetry - with a combined period running from 1992 to 2018 (Extended Data Figure 1). We also assess 6 model estimates of GIA (Extended Data Table 1) and 10 model estimates of SMB (Extended Data Table 2).

Drainage Basins

We analyse mass trends using two ice sheet drainage basin sets (Extended Data Figure 2), to allow consistency with those used in the first IMBIE assessment [1], and to evaluate an updated definition tailored towards mass budget assessments. The first set comprises 19 drainage basins delineated using surface elevation maps derived from ICESat-1 with a total area of 1,703,625 km [2,20]. The second drainage basin set is an updated definition considering other factors such as the direction of ice flow and includes 6 basins with a combined area of 1,723,300 km [2,37]. The two drainage basin sets differ by 1% in area at the scale of the Greenland Ice Sheet, and this has a negligible impact on mass trends when compared to the estimated uncertainty of individual techniques.

Glacial isostatic adjustment

GIA - the delayed response of Earth's interior to temporal changes in ice loading - affects estimates of ice sheet mass balance determined from satellite gravimetry and, to a lesser extent, satellite altimetry [51]. Here, we compare 6 independent models of GIA in the vicinity of the Greenland Ice Sheet (Extended Data Table 1). The GIA model solutions we did consider differ for a variety of reasons, including differences in their physics, in their computational approach, in their prescriptions of solid Earth unloading during the last glacial cycle and their Earth rheology, and in the data sets against which they are evaluated. Although alternative ice histories (e.g.[52]) and mantle viscosities (e.g.[53]) are available, we restricted our comparison to those contributed to our assessment. No approach is generally accepted as optimal, and so we evaluate the models by computing the mean and standard deviation of their predicted uplift rates (Extended Data Figure 3). We also estimate the contribution of each model to gravimetric mass trends using a common processing approach [41] which puts special emphasis on the treatment of low spherical harmonic degrees in the GIA-related trends in the gravitational field.

The highest rates of GIA-related uplift occur in northern Greenland - though this region also exhibits marked variability among the solutions, as does the area around Kangerlussuaq Glacier to the southeast. Even though the model spread is high in northern Greenland, the signal in this sector is also consistently high in most solutions. However, none of the GIA models considered here fully captures all areas of high uplift present in the models, and so it is possible there is a bias towards low values in the average field across the ice sheet overall. The models yield an average adjustment for GRACE estimates of Greenland Ice Sheet mass balance of -3 Gt/yr, with a standard deviation of around 20 Gt/yr. The spread is likely in part due to differences in the way each model accounts for GIA in North America which is ongoing and impacts western Greenland, and so care must be taken when estimating mass balance at basin scale. Local misrepresentation of the solid Earth response

548 can also have a relatively large impact stemming especially from lateral variations of solid-Earth
549 properties [42,54], and revisions of the current state of knowledge can be expected [34].

550 Surface mass balance

551 Here, ice-sheet SMB is defined as total precipitation minus sublimation, evaporation and meltwater
552 runoff, i.e. the interaction of the atmosphere and the superficial snow and firn layers, for example
553 through mass exchanges via precipitation, sublimation, and runoff, and through mass redistribution
554 by snowdrift, melting, and refreezing. We compare 10 estimates of Greenland Ice Sheet SMB derived
555 using a range of alternative approaches; 4 regional climate models (RCM's), 2 downscaled RCM's, a
556 global reanalysis, 2 downscaled model reanalyses of climate data, and 1 gridded model of snow
557 processes driven by climate model output (Extended Data Table 2).

558 Although SMB models of similar class tend to produce similar results, there are larger differences
559 between classes – most notably the global reanalysis and the process model which lead to estimates
560 of SMB that are significantly higher and lower than all other solutions, respectively. The regional
561 climate model solutions agree well at the scale of individual drainage sectors, with the largest
562 differences occurring in north-east Greenland (Extended Data Figure 4). The snow process model
563 tends to underestimate SMB when compared to the other solutions we have considered in various
564 sectors of the ice sheet, at times even yielding negative SMB, while the global reanalysis tends to
565 overestimate it.

566 Across all models, the average SMB of the Greenland Ice Sheet between 1980 to 2012 is 351 Gt/yr
567 and the standard deviation is 98 Gt/yr. However, the spread among the 8 RCM's and downscaled
568 reanalyses is considerably smaller; these solutions lead to an average Greenland Ice Sheet SMB of
569 361 Gt/yr with a standard deviation of 40 Gt/yr over the same period. By comparison, the global
570 reanalysis and process model lead to ice sheet wide estimates of SMB that are significantly larger
571 (504 Gt/yr) and smaller (125 Gt/yr) than this range, respectively. Model resolution is an important
572 factor when estimating SMB and its components, as respective contributions where only the spatial
573 resolution differed yield regional differences. Additionally, the underlying model domains were
574 identified as a source of discrepancy in the case of the Greenland Ice Sheet, as some products would
575 allocate the ablation area outside the given mask.

576 Individual estimates of ice sheet mass balance

577 To standardise our comparison and aggregation of the 26 individual satellite estimates of Greenland
578 Ice Sheet mass balance, we applied a common approach to derive rates of mass change from
579 cumulative mass trends [41]. Rates of mass change were computed over 36-month intervals centred
580 on regularly spaced (monthly) epochs within each cumulative mass trend time series, oversampling
581 the individual time series where necessary. At each epoch, rates of mass change were estimated by
582 fitting a linear trend to data within the surrounding 36-month time window using a weighted least-
583 squares approach, with each point weighted by its measurement error. The associated mass trend
584 uncertainties were estimated as the root sum square of the regression error and the measurement
585 error. Time series were truncated by half the moving-average window period at the start and end of
586 their period. The emerging rates of mass change were then averaged over 12-month periods to
587 reduce the impact of seasonal cycles.

588 **Gravimetry** We include 14 estimates of Greenland Ice Sheet ice sheet mass balance determined
589 from GRACE satellite gravimetry which together span the period 2003 to 2016 (Extended Data Figure
590 1). 10 of the gravimetry solutions were computed using spherical harmonic solutions to the global
591 gravity field and 4 were computed using spatially defined mass concentration units (Supplementary
592 Table 1). An unrestricted range of alternative GIA corrections were used in the formation of the

gravimetry mass balance solutions based on commonly-adopted model solutions and their variants [34,54–60] (Supplementary Table 1). All of the gravimetry mass balance solutions included in this study use the same degree-1 coefficients to account for geocenter motion [61] and, although an alternative set is now available [62], the estimated improvement in certainty is small in comparison to their magnitude and spread. There was some variation in the sampling of the individual gravimetry data sets, and their collective effective (weighted mean) temporal resolution is 0.08 years. Overall, there is good agreement between rates of Greenland Ice Sheet mass change derived from satellite gravimetry (Extended Data Figure 5); all solutions show the ice sheet to be in a state of negative mass balance throughout their survey periods, with mass loss peaking in 2011 and reducing thereafter. During the period 2005 to 2015, annual rates of mass change determined from satellite gravimetry differ by 97 Gt/yr on average, and their average standard deviation is 30 Gt/yr (Extended Data Table 3).

Altimetry We include 9 estimates of Greenland Ice Sheet mass balance determined from satellite altimetry which together span the period 2004 to 2018 (Extended Data Figure 1). 3 of the solutions are derived from radar altimetry, 4 from laser altimetry, and 2 use a combination of both (Supplementary Table 1). The altimetry mass trends are also computed using a range of approaches, including crossovers, planar fits, and repeat track analyses. The laser altimetry mass trends are computed from ICESat-1 data as constant rates of mass change over their respective survey periods, while the radar altimetry mass trends are computed from EnviSat and/or CryoSat-2 data with a temporal resolution of between 1 and 72 months. In consequence, the altimetry solutions have an effective collective temporal resolution of 0.74 years. Mass changes are computed after making corrections for alternative sources of surface elevation change, including glacial isostatic and elastic adjustment, and firn height changes (see Supplementary Table 1). Despite the range of input data and technical approaches, there is good overall agreement between rates of mass change determined from the various satellite altimetry solutions (Extended Data Figure 5). All altimetry solutions show the Greenland Ice Sheet to be in a state of negative mass balance throughout their survey periods, with mass loss peaking in 2012 and reducing thereafter. During the period 2005 to 2015, annual rates of mass change determined from satellite altimetry differ by 111 Gt/yr on average, and, their average standard deviation is 40 Gt/yr (Extended Data Table 3). The greatest variance lies among the 4 laser altimetry mass balance solutions which range from -248 to -128 Gt/yr between 2004 and 2010; aside from methodological differences, possible explanations for this high spread include the relatively short period over which the mass trends are determined, the poor temporal resolution of these data sets, and the rapid change in mass balance occurring during the period in question.

Input-Output Method We include 3 estimates of Greenland Ice Sheet mass balance determined from the input-output method which together span the period 1992 to 2015 (Extended Data Figure 1). Although there are relatively few data sets by comparison to the gravimetry and altimetry solutions, the input-output data provide information on the partitioning of the mass change (surface processes and/or ice dynamics) cover a significantly longer period and are therefore an important record of changes in Greenland Ice Sheet mass during the 1990's. The input-output method makes use of a wide range of satellite imagery (e.g. [6,40,63–68]) combined with measurements of ice thickness (e.g. [69]) for computing ice sheet discharge (output), and several alternative SMB model estimates of snow accumulation (input) and runoff (output) (see Supplementary Table 1). 2 of the input-output method datasets exhibit temporal variability across their survey periods, and 2 provide only constant rates of mass changes. Although these latter records are relatively short, they are an important marker with which variances among independent estimates can be evaluated. The collective effective (weighted mean) temporal resolution of the input-output method data is 0.14 years,

although it should be noted that in earlier years the satellite ice discharge component of the data are relatively sparsely sampled in time (e.g. [70]).There is good overall agreement between rates of mass change determined from the input-output method solutions (Extended Data Figure 5). During the period 2005 to 2015, annual rates of mass change determined from the 4 input-output data sets differ by up to 47 Gt/yr on average, and their average standard deviation is 22 Gt/yr (Extended Data Table 3). These differences are comparable to the estimated uncertainty of the individual techniques and are also small relative to the estimated mass balance over the period in question. In addition to showing that the Greenland Ice Sheet was in a state of negative mass balance since 2000, with mass loss peaking in 2012 and reducing thereafter, the input-output method data show that the ice sheet was close to a state of balance prior to this period [33].

Aggregate estimate of ice sheet mass balance

To produce an aggregate estimate of Greenland Ice Sheet mass balance, we combine the 14 gravimetry, 9 altimetry, and 3 input-output method datasets to produce a single 26-year record spanning the period 1992 to 2018. First, we combine the gravimetry, altimetry, and the input-output method data separately into three time-series by forming an error-weighted average of individual rates of ice sheet mass change computed using the same technique (Extended Data Figure 6). At each epoch, we estimate the uncertainty of these time-series as the root mean square of their component time-series errors. We then combine the mass balance time-series derived from gravimetry, altimetry, and the input-output method to produce a single, aggregate (reconciled) estimate, computed as the error-weighted mean of mass trends sampled at each epoch. We estimated the uncertainty of this reconciled rate of mass balance as either the root mean square departure of the constituent mass trends from their weighted-mean or the root mean square of their uncertainties, whichever is larger, divided by the square root of the number of independent satellite techniques used to form the aggregate. Cumulative uncertainties are computed as the root sum square of annual errors, on the assumption that annual errors are not correlated over time. This assumption has been employed in numerous mass balance studies [1,17,33,41], and its effect is to reduce cumulative errors by a factor 2.2 over the 5-year periods we employ in this study (Table 1). If some sources of error are temporally correlated, the cumulative uncertainty may therefore be underestimated. In a recent study, for example, it is estimated that 30 % of the annual mass balance error is systematic [71], and in this instance the cumulative error may be 37 % larger. On the other hand, the estimated annual error on aggregate mass trends reported in this study (61 Gt/yr) are 70% larger than the spread of the independent estimates from which they are combined (36 Gt/yr) (Extended Data Table 3), which suggests the underlying errors may be overestimated by a similar degree. A more detailed analysis of the measurement and systematic errors is required to improve the cumulative error budget.

During the period 2004 to 2015, when all three satellite techniques were in operation, there is good agreement between changes in ice sheet mass balance on a variety of timescales (Extended Data Figure 6). In Greenland, there are large annual cycles in mass superimposed on equally prominent interannual fluctuations as well as variations of intermediate (~5 years) duration. These signals are consistent with fluctuations in SMB that have been identified in meteorological records [1,72], and are present within the time-series of mass balance emerging from all three satellite techniques, to varying degrees, according to their effective temporal resolution. For example, correlated seasonal cycles are apparent in the gravimetry and input-output method mass balance time series, because their effective temporal resolutions are sufficiently short (0.08 and 0.14 years, respectively) to resolve such changes. However, at 0.74 years, the effective temporal resolution of the altimetry mass balance time series is too coarse to detect cycles on sub-annual timescales. Nevertheless,

when the aggregated mass balance data emerging from all three experiment groups are degraded to a common temporal resolution of 36 months, the time-series are well correlated ($0.63<r^2<0.80$) and, over longer periods, all techniques identify the marked increases in Greenland Ice Sheet mass loss peaking in 2012. During the period 2005 to 2015, annual rates of mass change determined from all three techniques differ by up 148 Gt/yr on average, and their average standard deviation is 39 Gt/yr - a value that is small when compared to their estimated uncertainty (63 Gt/yr)(Extended Data Table 3).

Methods References

51. Wahr, J., Wingham, D. & Bentley, C. A method of combining ICESat and GRACE satellite data to constrain Antarctic mass balance. *Journal of Geophysical Research: Solid Earth* **105**, 16279–16294 (2000).
52. Lambeck, K., Rouby, H., Purcell, A., Sun, Y. & Sambridge, M. Closing the sea level budget at the Last Glacial Maximum. *PNAS* **111**, 15861–15862 (2014).
53. Caron, L., Métivier, L., Greff-Lefftz, M., Fleitout, L. & Rouby, H. Inverting Glacial Isostatic Adjustment signal using Bayesian framework and two linearly relaxing rheologies. *Geophys J Int* **209**, 1126–1147 (2017).
54. Peltier, W. R., Argus, D. F. & Drummond, R. Space geodesy constrains ice age terminal deglaciation: The global ICE-6G_C (VM5a) model. *Journal of Geophysical Research: Solid Earth* **120**, 450–487 (2015).
55. Paulson, A., Zhong, S. & Wahr, J. Inference of mantle viscosity from GRACE and relative sea level data. *Geophys J Int* **171**, 497–508 (2007).
56. Peltier, W. R. Global Glacial Isostasy and the Surface of the Ice-Age Earth: The ICE-5G (VM2) Model and GRACE. *Annual Review of Earth and Planetary Sciences* **32**, 111–149 (2004).
57. Simpson, M. J. R., Milne, G. A., Huybrechts, P. & Long, A. J. Calibrating a glaciological model of the Greenland ice sheet from the Last Glacial Maximum to present-day using field observations of relative sea level and ice extent. *Quaternary Science Reviews* **28**, 1631–1657 (2009).

58. A, G., Wahr, J. & Zhong, S. Computations of the viscoelastic response of a 3-D compressible Earth to surface loading: an application to Glacial Isostatic Adjustment in Antarctica and Canada. *Geophys J Int* **192**, 557–572 (2013).
59. Schrama, E. J. O., Wouters, B. & Rietbroek, R. A mascon approach to assess ice sheet and glacier mass balances and their uncertainties from GRACE data. *Journal of Geophysical Research: Solid Earth* **119**, 6048–6066 (2014).
60. Klemann, V. & Martinec, Z. Contribution of glacial-isostatic adjustment to the geocenter motion. *Tectonophysics* **511**, 99–108 (2011).
61. Swenson, S., Chambers, D. & Wahr, J. Estimating geocenter variations from a combination of GRACE and ocean model output. *Journal of Geophysical Research: Solid Earth* **113**, (2008).
62. Sun, Y., Riva, R. & Ditmar, P. Optimizing estimates of annual variations and trends in geocenter motion and J2 from a combination of GRACE data and geophysical models. *Journal of Geophysical Research: Solid Earth* **121**, 8352–8370 (2016).
63. Nagler, T., Rott, H., Hetzenecker, M., Wuite, J. & Potin, P. The Sentinel-1 Mission: New Opportunities for Ice Sheet Observations. *Remote Sensing* **7**, 9371–9389 (2015).
64. Mouginot, J., Rignot, E., Scheuchl, B. & Millan, R. Comprehensive Annual Ice Sheet Velocity Mapping Using Landsat-8, Sentinel-1, and RADARSAT-2 Data. *Remote Sensing* **9**, 364 (2017).
65. Joughin, I., Smith, B. E. & Howat, I. Greenland Ice Mapping Project: ice flow velocity variation at sub-monthly to decadal timescales. *The Cryosphere* **12**, 2211–2227 (2018).
66. Lemos, A. *et al.* Ice velocity of Jakobshavn Isbræ, Petermann Glacier, Nioghalvfjerdsfjorden, and Zachariæ Isstrøm, 2015–2017, from Sentinel 1-a/b SAR imagery. *The Cryosphere* **12**, 2087–2097 (2018).
67. Joughin, I. *et al.* Continued evolution of Jakobshavn Isbrae following its rapid speedup. *Journal of Geophysical Research: Earth Surface* **113**, (2008).
68. Joughin, I., Abdalati, W. & Fahnestock, M. Large fluctuations in speed on Greenland's Jakobshavn Isbræ glacier. *Nature* **432**, 608–610 (2004).

69. Gogineni, S. *et al.* Coherent radar ice thickness measurements over the Greenland ice sheet. *Journal of Geophysical Research: Atmospheres* **106**, 33761–33772 (2001).
70. Rignot, E. *et al.* Recent Antarctic ice mass loss from radar interferometry and regional climate modelling. *Nature Geosci* **1**, 106–110 (2008).
71. Shepherd, A. *et al.* Trends in Antarctic Ice Sheet Elevation and Mass. *Geophysical Research Letters* **46**, 8174–8183 (2019).
72. Wouters, B., Bamber, J. L., van den Broeke, M. R., Lenaerts, J. T. M. & Sasgen, I. Limits in detecting acceleration of ice sheet mass loss due to climate variability. *Nature Geoscience* **6**, 613–616 (2013).
73. Rignot, E., Mouginot, J. & Scheuchl, B. Ice Flow of the Antarctic Ice Sheet. *Science* **333**, 1427–1430 (2011).
74. Rignot, E., Mouginot, J. & Scheuchl, B. Antarctic grounding line mapping from differential satellite radar interferometry. *Geophysical Research Letters* **38**, (2011).
75. Langen, P. L., Fausto, R. S., Vandecrux, B., Mottram, R. H. & Box, J. E. Liquid Water Flow and Retention on the Greenland Ice Sheet in the Regional Climate Model HIRHAM5: Local and Large-Scale Impacts. *Front. Earth Sci.* **4**, (2017).
76. Martinec, Z. & Hagedoorn, J. The rotational feedback on linear-momentum balance in glacial isostatic adjustment. *Geophys J Int* **199**, 1823–1846 (2014).
77. Fretwell, P. *et al.* Bedmap2: improved ice bed, surface and thickness datasets for Antarctica. *The Cryosphere* **7**, 375–393 (2013).
78. Martinec, Z. Spectral–finite element approach to three-dimensional viscoelastic relaxation in a spherical earth. *Geophys J Int* **142**, 117–141 (2000).
79. Fleming, K. & Lambeck, K. Constraints on the Greenland Ice Sheet since the Last Glacial Maximum from sea-level observations and glacial-rebound models. *Quaternary Science Reviews* **23**, 1053–1077 (2004).

80. King, M. A., Whitehouse, P. L. & van der Wal, W. Incomplete separability of Antarctic plate rotation from glacial isostatic adjustment deformation within geodetic observations. *Geophys J Int* **204**, 324–330 (2016).
81. Spada, G., Melini, D. & Colleoni, F. *Computational Infrastructure for Geodynamics*. (2018).
82. Noël, B. *et al.* Evaluation of the updated regional climate model RACMO2.3: summer snowfall impact on the Greenland Ice Sheet. *The Cryosphere* **9**, 1831–1844 (2015).
83. Noël, B. *et al.* A daily, 1 km resolution data set of downscaled Greenland ice sheet surface mass balance (1958–2015). *The Cryosphere* **10**, 2361–2377 (2016).
84. Gelaro, R. *et al.* The Modern-Era Retrospective Analysis for Research and Applications, Version 2 (MERRA-2). *J. Climate* **30**, 5419–5454 (2017).
85. Wilton, D. J. *et al.* High resolution (1 km) positive degree-day modelling of Greenland ice sheet surface mass balance, 1870–2012 using reanalysis data. *Journal of Glaciology* **63**, 176–193 (2017).
86. Mernild, S. H., Liston, G. E., Hiemstra, C. A. & Christensen, J. H. Greenland Ice Sheet Surface Mass-Balance Modeling in a 131-Yr Perspective, 1950–2080. *J. Hydrometeor.* **11**, 3–25 (2010).
87. Bonin, J. & Chambers, D. Uncertainty estimates of a GRACE inversion modelling technique over Greenland using a simulation. *Geophys J Int* **194**, 212–229 (2013).
88. Blazquez, A. *et al.* Exploring the uncertainty in GRACE estimates of the mass redistributions at the Earth surface: implications for the global water and sea level budgets. *Geophys J Int* **215**, 415–430 (2018).
89. Forsberg, R., Sørensen, L. & Simonsen, S. Greenland and Antarctica Ice Sheet Mass Changes and Effects on Global Sea Level. *Surv Geophys* **38**, 89–104 (2017).
90. Groh, A. & Horwath, M. The method of tailored sensitivity kernels for GRACE mass change estimates. in (2016).
91. Harig, C. & Simons, F. J. Mapping Greenland's mass loss in space and time. *PNAS* **109**, 19934–19937 (2012).

92. Luthcke, S. B. *et al.* Antarctica, Greenland and Gulf of Alaska land-ice evolution from an iterated GRACE global mascon solution. *Journal of Glaciology* **59**, 613–631 (2013).

93. Andrews, S. B., Moore, P. & King, M. A. Mass change from GRACE: a simulated comparison of Level-1B analysis techniques. *Geophys J Int* **200**, 503–518 (2015).

94. Save, H., Bettadpur, S. & Tapley, B. D. High-resolution CSR GRACE RL05 mascons. *Journal of Geophysical Research: Solid Earth* **121**, 7547–7569 (2016).

95. Seo, K.-W. *et al.* Surface mass balance contributions to acceleration of Antarctic ice mass loss during 2003–2013. *Journal of Geophysical Research: Solid Earth* **120**, 3617–3627 (2015).

96. Velicogna, I., Sutterley, T. C. & Broeke, M. R. van den. Regional acceleration in ice mass loss from Greenland and Antarctica using GRACE time-variable gravity data. *Geophysical Research Letters* **41**, 8130–8137 (2014).

97. Vishwakarma, B. D., Horwath, M., Devaraju, B., Groh, A. & Sneeuw, N. A Data-Driven Approach for Repairing the Hydrological Catchment Signal Damage Due to Filtering of GRACE Products. *Water Resources Research* **53**, 9824–9844 (2017).

98. Wiese, D. N., Landerer, F. W. & Watkins, M. M. Quantifying and reducing leakage errors in the JPL RL05M GRACE mascon solution. *Water Resources Research* **52**, 7490–7502 (2016).

99. Ivins, E. R. & James, T. S. Antarctic glacial isostatic adjustment: a new assessment. *Antarctic Science* **17**, 541–553 (2005).

100. Ivins, E. R. *et al.* Antarctic contribution to sea level rise observed by GRACE with improved GIA correction. *Journal of Geophysical Research: Solid Earth* **118**, 3126–3141 (2013).

101. Klemann, V. & Martinec, Z. Contribution of glacial-isostatic adjustment to the geocenter motion. *Tectonophysics* **511**, 99–108 (2011).

102. Rodell, M. *et al.* The Global Land Data Assimilation System. *Bull. Amer. Meteor. Soc.* **85**, 381–394 (2004).

103. Döll, P., Kaspar, F. & Lehner, B. A global hydrological model for deriving water availability indicators: model tuning and validation. *Journal of Hydrology* **270**, 105–134 (2003).

104. Cheng, M., Tapley, B. D. & Ries, J. C. Deceleration in the Earth's oblateness. *Journal of Geophysical Research: Solid Earth* **118**, 740–747 (2013).

105. Balmaseda, M. A., Mogensen, K. & Weaver, A. T. Evaluation of the ECMWF ocean reanalysis system ORAS4. *Quarterly Journal of the Royal Meteorological Society* **139**, 1132–1161 (2013).

106. Pujol, M.-I. *et al.* DUACS DT2014: the new multi-mission altimeter data set reprocessed over 20 years. *Ocean Science* **12**, 1067–1090 (2016).

107. Menemenlis, D. *et al.* ECCO2: High Resolution Global Ocean and Sea Ice Data Synthesis. *AGU Fall Meeting Abstracts* **2008**, OS31C-1292 (2008).

108. Dobslaw, H. *et al.* Simulating high-frequency atmosphere-ocean mass variability for dealiasing of satellite gravity observations: AOD1B RL05. *Journal of Geophysical Research: Oceans* **118**, 3704–3711 (2013).

109. Carrère, L. & Lyard, F. Modeling the barotropic response of the global ocean to atmospheric wind and pressure forcing - comparisons with observations. *Geophysical Research Letters* **30**, (2003).

110. Csatho, B. M. *et al.* Laser altimetry reveals complex pattern of Greenland Ice Sheet dynamics. *PNAS* **111**, 18478–18483 (2014).

111. Nilsson, J., Gardner, A., Sandberg Sørensen, L. & Forsberg, R. Improved retrieval of land ice topography from CryoSat-2 data and its impact for volume-change estimation of the Greenland Ice Sheet. *The Cryosphere* **10**, 2953–2969 (2016).

112. Gourmelen, N. *et al.* CryoSat-2 swath interferometric altimetry for mapping ice elevation and elevation change. *Advances in Space Research* **62**, 1226–1242 (2018).

113. Gunter, B. C. *et al.* Empirical estimation of present-day Antarctic glacial isostatic adjustment and ice mass change. *The Cryosphere* **8**, 743–760 (2014).

114. Helm, V., Humbert, A. & Miller, H. Elevation and elevation change of Greenland and Antarctica derived from CryoSat-2. *The Cryosphere* **8**, 1539–1559 (2014).

115. Kjeldsen, K. K. *et al.* Improved ice loss estimate of the northwestern Greenland ice sheet. *Journal of Geophysical Research: Solid Earth* **118**, 698–708 (2013).

116. Felikson, D. *et al.* Comparison of Elevation Change Detection Methods From ICESat Altimetry Over the Greenland Ice Sheet. *IEEE Transactions on Geoscience and Remote Sensing* **55**, 5494–5505 (2017).

117. Andersen, M. L. *et al.* Basin-scale partitioning of Greenland ice sheet mass balance components (2007–2011). *Earth and Planetary Science Letters* **409**, 89–95 (2015).

118. Colgan, W. *et al.* Greenland ice sheet mass balance assessed by PROMICE (1995–2015). *Geological Survey of Denmark and Greenland Bulletin* **43**, (2019).

119. van Wessem, J. M. *et al.* Updated cloud physics in a regional atmospheric climate model improves the modelled surface energy balance of Antarctica. *The Cryosphere* **8**, 125–135 (2014).

120. Fettweis, X. *et al.* Estimating the Greenland ice sheet surface mass balance contribution to future sea level rise using the regional atmospheric climate model MAR. *The Cryosphere* **7**, 469–489 (2013).

Data availability

The aggregated Greenland Ice Sheet mass-balance data and estimated errors generated in this study are freely available at http://imbie.org and at the NERC Polar Data Centre. The code used to compute and aggregate rates of ice sheet mass change and their estimated errors are freely available at https://github.com/IMBIE.

Extended Data Legends

Extended Data Figure 1 | Ice sheet mass balance data sets. Participant datasets used in this study and their main contributors (a, top) and the number and class of data available in each calendar year (b, bottom). The interval 2003 to 2010 includes almost all datasets and is selected as the overlap period. Further details of the satellite observations used in this study are provided in Supplementary Table 1.

Extended Data Figure 2 | Greenland Ice Sheet drainage basins. Basin used in this study, according to the definitions of ref [20] (a, left) and ref [37] (b, right).

Extended Data Figure 3 | Modelled glacial isostatic adjustment in Greenland. Bedrock uplift rates in Greenland averaged over the glacial isostatic adjustment (GIA) model solutions used in this study (a, left), as well as their standard deviation (b, right). Further details of the GIA models used in this study are provided in Extended Data Table 1. High rates of uplift and subsidence associated with the former Laurentide Ice Sheet are apparent to the southwest of Greenland.

Extended Data Figure 4 | Surface mass balance of the Greenland Ice Sheet. Time series of surface mass balance (SMB) in (a) NW, (b) SW, (c) NE, (d) CW, (e) SE and (f) NO Greenland Ice Sheet drainage basins (Extended Data Figure 2) [73,74]. Solid lines are annual averages of the monthly data (dashed lines). Further details of the SMB models used in this study are provided in Extended Data Table 2.

Extended Data Figure 5 | Greenland Ice Sheet mass balance intra-comparison. Individual rates of Greenland ice-sheet mass balance used in this study as determined from satellite altimetry (a, top), gravimetry (b, centre) and the input–output method (c, bottom). The light-grey shading shows the estimated 1σ uncertainty relative to the ensemble average. The standard error of the mean solutions, per epoch, is shown in mid-grey.

Extended Data Figure 6 | Greenland Ice Sheet mass balance inter-comparison. Rate of Greenland Ice Sheet mass balance as derived from the three techniques of satellite radar and laser altimetry (red), input-output method (blue), and gravimetry (green), and their arithmetic mean (gray). The estimated uncertainty is also shown (light shading) and is computed as the root mean square of the component time-series errors.

Extended Data Figure 7 | Cumulative Greenland Ice Sheet surface mass balance. The cumulative surface mass change (lightest blue) determined from an average of the RACMO2.3p2 [46] (light blue), MARv3.6 [21] (mid-blue) and HIRHAM [9] (dark blue) regional climate models relative to their 1980-1990 means (see Methods). The estimated uncertainty of the average change is also shown (shaded area) is computed as the average of the uncertainties from each of the three models. RACMO2.3p2 uncertainties are based upon a comparison to in-situ observations [33]. MARv3.6 uncertainties are evaluated from the variability due to forcing from climate reanalyses [21]. HIRHAM uncertainties are estimated based on comparisons to in-situ accumulation and ablation data [75]. Cumulative uncertainties are computed as the root sum square of annual errors, on the assumption that these errors are not correlated over time [17].

Extended Data Table 1. Glacial Isostatic Adjustment models. Details of Glacial Isostatic Adjustment (GIA) models used in this study.

†Regional changes in mass associated with the GIA signal determined by the contributor.
‡Regional changes in mass associated with the GIA signal calculated as an indicative rate using spherical-harmonic degrees 3 to 90 and a common treatment of degree 2 [76].
[a] Main reference publication(s).
[b] Model from main publication unless otherwise stated. Comma-separated values refer to properties of a radially varying (1D, one-dimensional) Earth model: the first value is lithosphere thickness (km), other values reflect mantle viscosity (x 10^{21} Pa s) for specific layers; see relevant publication.
[c] GIA model details: SH=spherical harmonic (maximum degree indicated), FE=finite element, C=compressible, IC=incompressible, RF=rotational feedback, SG=self-gravitation, OL=ocean loading, 'x' = feature not included.
[d] RSL = relative sea-level data; GPS rates corrected for elastic response to contemporary ice mass change.
[e] Earth model taken from ref [54]
[f] Ice model taken from ref [54]
[g] Different to ICE-6G_C in Antarctica, owing to the use of BEDMAP2 [77] topography.

Extended Data Table 2. Surface mass balance models. Details of the surface mass balance (SMB) models used in this study. [a] Main reference publication; additional references are provided in Supplementary Table 1. [b] SMB model class; regional climate model (RCM), global numerical analysis (GA), process model (PM). Native resolution (n) and downscaled (d) models are also identified. [c] Averages over the period 1980 to 2012 for the Greenland Ice Sheet excluding peripheral ice caps and using the drainage basins from ref [37].

Extended Data Table 3: Rate of Greenland Ice Sheet mass change, 2005-2015. Estimates of ice-sheet mass balance from satellite altimetry, gravimetry the input–output method, and from all three groups during the period 2005 to 2015. Also shown are the average standard deviations (s.d.) and ranges of individual estimates within each group during the same period.
*No altimetry data in 2010.

941

Altimetry

Surface

1.00
0.75
0.50
0.25
0.00
−0.25
−0.50
−0.75
−1.00
m/year

1992-1997 1997-2002 2002-2007 2007-2012 2012-2017

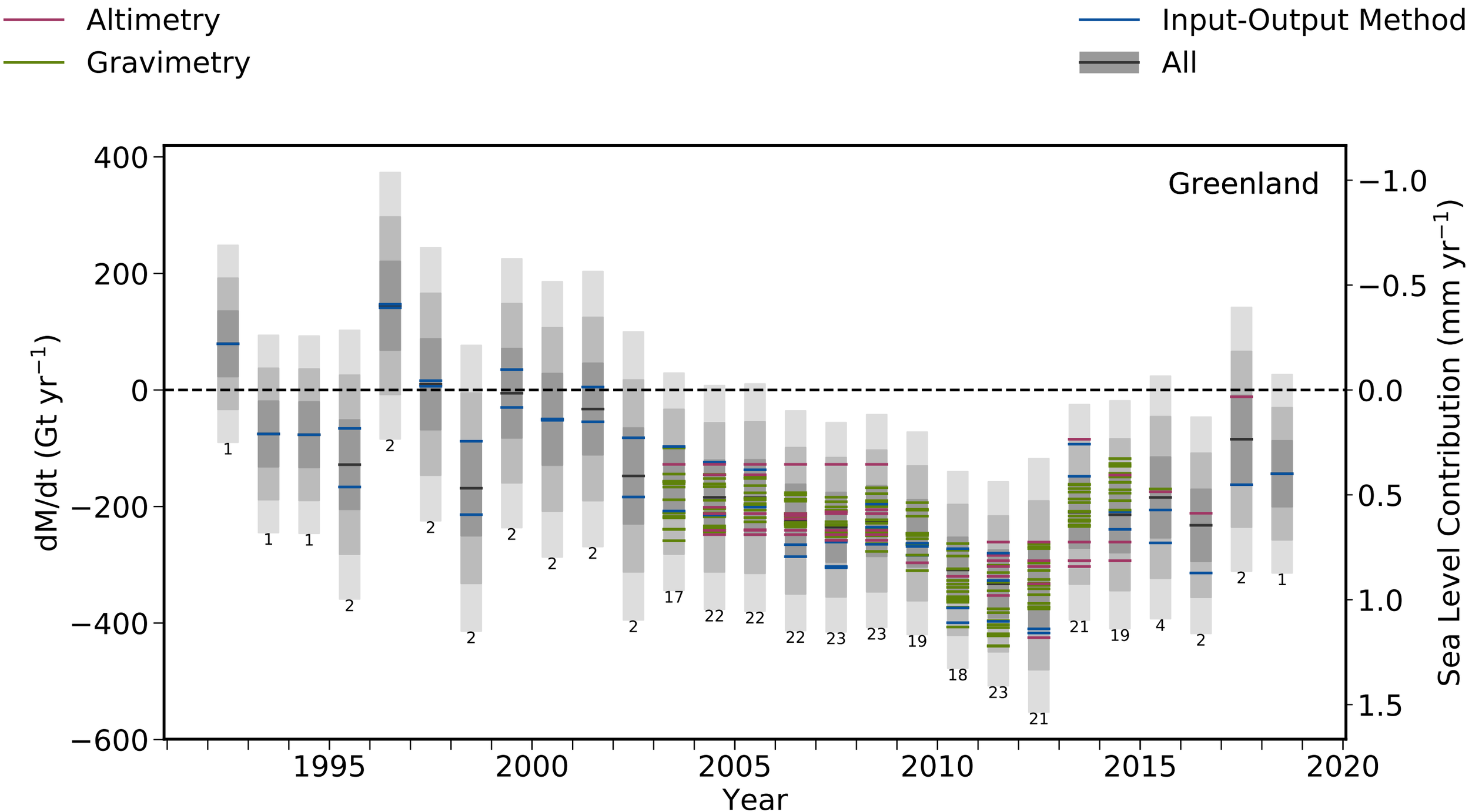
Altimetry
Gravimetry
Input-Output Method
All
Greenland
dM/dt (Gt yr^{-1})
Sea Level Contribution (mm yr^{-1})
Year
400
200
0
−200
−400
−600
−1.0
−0.5
0.0
0.5
1.0
1.5
1995
2000
2005
2010
2015
2020
1
1
1
2
2
2
2
2
2
2
2
17
22
22
22
23
23
19
18
23
21
21
19
4
2
2
1

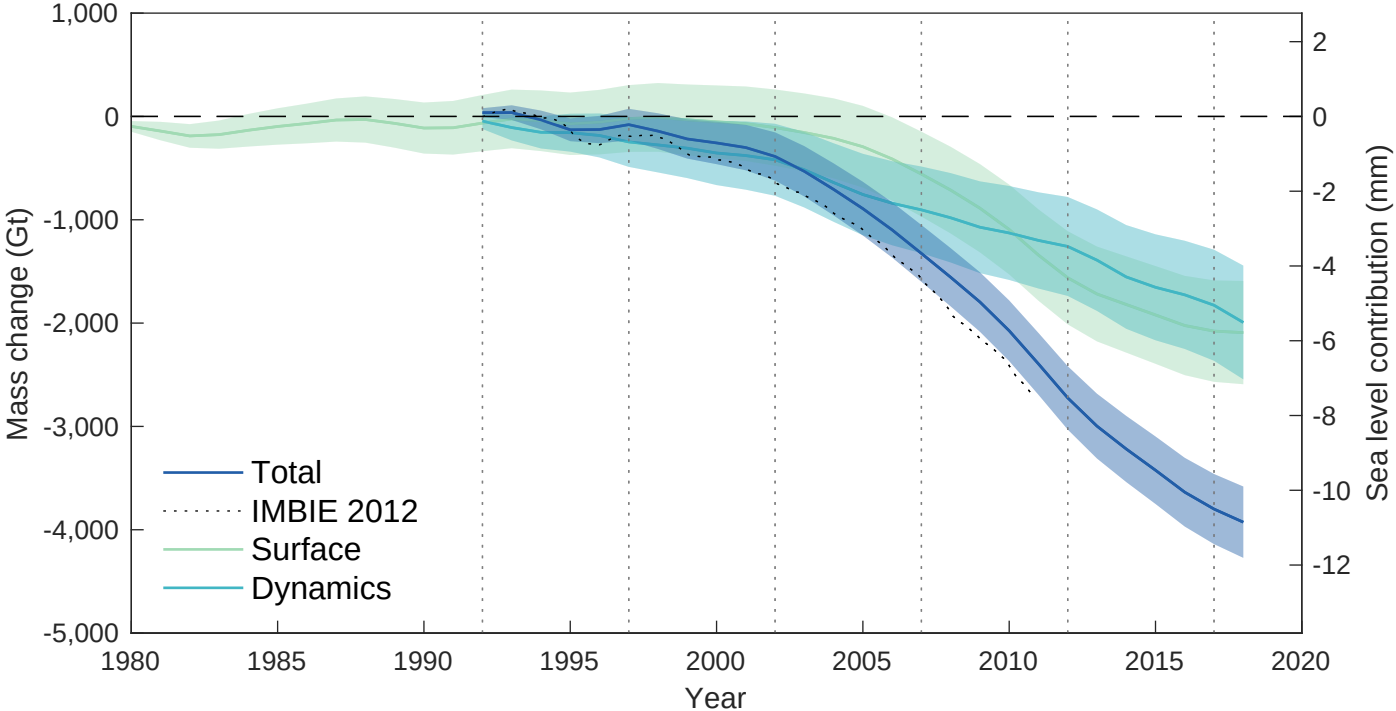
1,000
0
-1,000
-2,000
-3,000
-4,000
-5,000
Mass change (Gt)
2
0
-2
-4
-6
-8
-10
-12
Sea level contribution (mm)
1980
1985
1990
1995
2000
2005
2010
2015
2020
Year
Total
IMBIE 2012
Surface
Dynamics

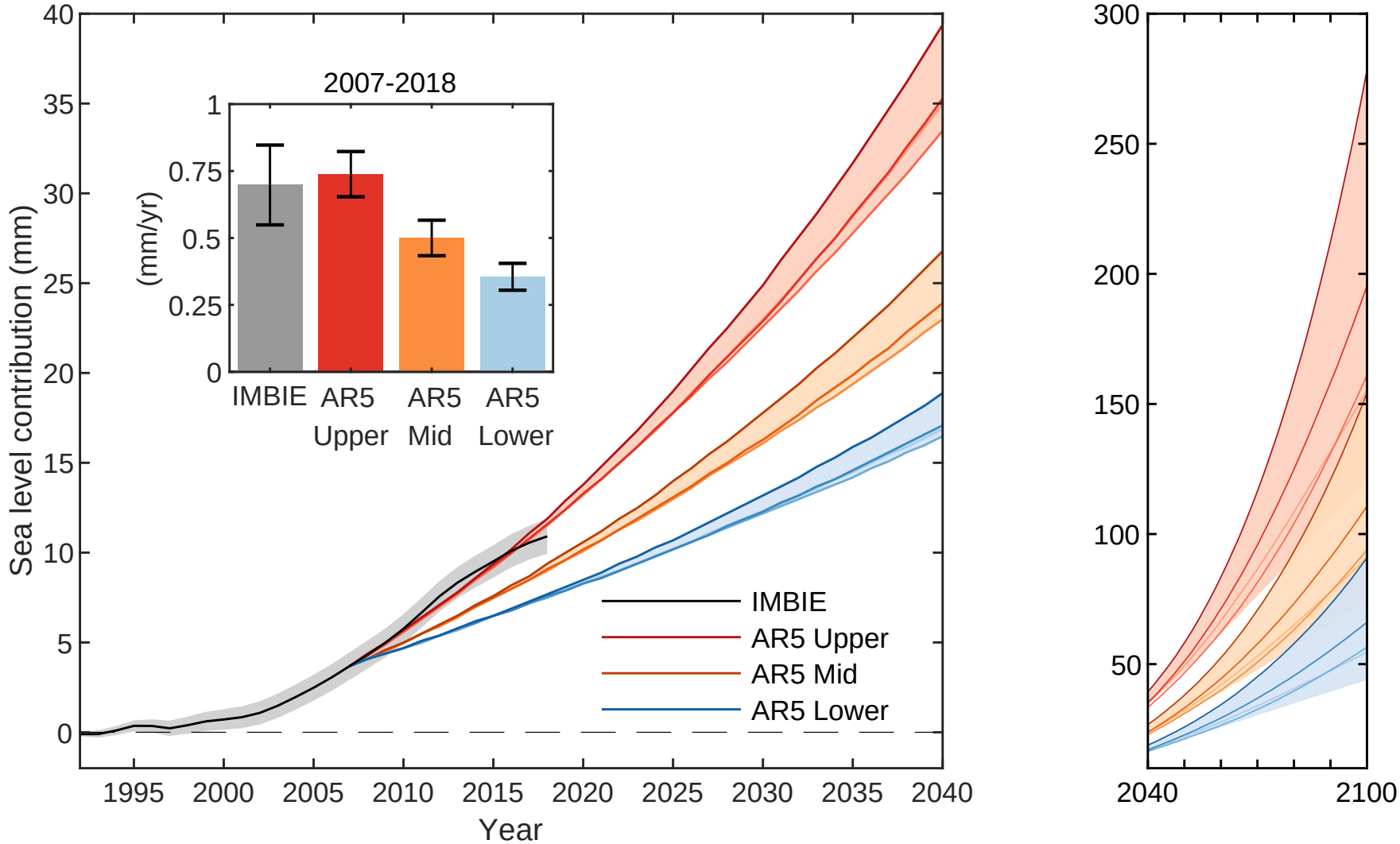
Sea level contribution (mm)
Year
2007-2018
(mm/yr)
IMBIE
AR5 Upper
AR5 Mid
AR5 Lower
IMBIE
AR5 Upper
AR5 Mid
AR5 Lower